OXFORD

Human Molecular Genetics, 2023, Vol. 32, 13, 2192–2204
https://doi.org/10.1093/hmg/ddad048
Advance access publication date 3 April 2023
Original Article

Pathogenic *SCN2A* variants cause early-stage dysfunction in patient-derived neurons

R. Asadollahi[1,2,†], I. Delvendahl[3,4,†], R. Muff[1], G. Tan[5], D.G. Rodríguez[5], S. Turan[6], M. Russo[1], B. Oneda[1], P. Joset[1], P. Boonsawat[1], R. Masood[1], M. Mocera[1], I. Ivanovski[1], A. Baumer[1], R. Bachmann-Gagescu[1], R. Schlapbach[5], H. Rehrauer[5], K. Steindl[1], A. Begemann[1], A. Reis[7], J. Winkler[8,9], B. Winner[6,9], M. Müller[3,4,10,11,†] and A. Rauch[1,4,10,11,12,13,14,†*]

[1]Institute of Medical Genetics, University of Zurich, Schlieren-Zurich 8952, Switzerland
[2]Faculty of Engineering and Science, University of Greenwich London, Medway Camplus, Chatham Maritime ME4 4TB, UK
[3]Department of Molecular Life Sciences, University of Zurich, Zurich 8057, Switzerland
[4]Neuroscience Center Zurich, University of Zurich, Zurich 8057, Switzerland
[5]Functional Genomics Center Zurich, ETH Zurich and University of Zurich, Zurich 8057, Switzerland
[6]Department of Stem Cell Biology, Friedrich-Alexander-Universität Erlangen-Nürnberg, Erlangen 91054, Germany,
[7]Institute of Human Genetics, Friedrich-Alexander-Universität Erlangen-Nürnberg, Erlangen 91054, Germany
[8]Department of Molecular Neurology, Friedrich-Alexander-Universität Erlangen-Nürnberg, Erlangen 91054, Germany
[9]Center for Rare Diseases Erlangen, University Hospital Erlangen, Erlangen 91054, Germany
[10]University of Zurich Clinical Research Priority Program (CRPP) Praeclare – Personalized prenatal and reproductive medicine, Zurich 8006, Switzerland
[11]University of Zurich Research Priority Program (URPP) AdaBD: Adaptive Brain Circuits in Development and Learning, Zurich 8006, Switzerland
[12]University of Zurich Research Priority Program (URPP) ITINERARE: Innovative Therapies in Rare Diseases, Zurich 8006, Switzerland
[13]Zurich Center for Integrative Human Physiology, University of Zurich, Zurich 8057, Switzerland and
[14]University Children's Hospital Zurich, University of Zurich, Zurich 8032, Switzerland
*To whom correspondence should be addressed at: Institute of Medical Genetics, University of Zurich, Wagistrasse 12, Schlieren-Zurich 8952, Switzerland. Tel: +41 (44) 5563300; Email: anita.rauch@medgen.uzh.ch
†These authors contributed equally.

Abstract

Pathogenic heterozygous variants in *SCN2A*, which encodes the neuronal sodium channel $Na_V1.2$, cause different types of epilepsy or intellectual disability (ID)/autism without seizures. Previous studies using mouse models or heterologous systems suggest that $Na_V1.2$ channel gain-of-function typically causes epilepsy, whereas loss-of-function leads to ID/autism. How altered channel biophysics translate into patient neurons remains unknown. Here, we investigated iPSC-derived early-stage cortical neurons from ID patients harboring diverse pathogenic *SCN2A* variants [p.(Leu611Valfs*35); p.(Arg937Cys); p.(Trp1716*)] and compared them with neurons from an epileptic encephalopathy (EE) patient [p.(Glu1803Gly)] and controls. ID neurons consistently expressed lower $Na_V1.2$ protein levels. In neurons with the frameshift variant, $Na_V1.2$ mRNA and protein levels were reduced by ~50%, suggesting nonsense-mediated decay and haploinsufficiency. In other ID neurons, only protein levels were reduced implying $Na_V1.2$ instability. Electrophysiological analysis revealed decreased sodium current density and impaired action potential (AP) firing in ID neurons, consistent with reduced $Na_V1.2$ levels. In contrast, epilepsy neurons displayed no change in $Na_V1.2$ levels or sodium current density, but impaired sodium channel inactivation. Single-cell transcriptomics identified dysregulation of distinct molecular pathways including inhibition of oxidative phosphorylation in neurons with *SCN2A* haploinsufficiency and activation of calcium signaling and neurotransmission in epilepsy neurons. Together, our patient iPSC-derived neurons reveal characteristic sodium channel dysfunction consistent with biophysical changes previously observed in heterologous systems. Additionally, our model links the channel dysfunction in ID to reduced $Na_V1.2$ levels and uncovers impaired AP firing in early-stage neurons. The altered molecular pathways may reflect a homeostatic response to $Na_V1.2$ dysfunction and can guide further investigations.

Introduction

SCN2A encodes the voltage-gated sodium channel $Na_V1.2$, which is widely expressed in the human central nervous system including excitatory cortical neurons (1–3). $Na_V1.2$ channels open, inactivate and close in response to membrane potential changes to control the influx of sodium ions, thereby regulating neuronal APs.

At the neonatal and early stages of life, $Na_V1.2$ serves as the main sodium channel for AP initiation and propagation. At about 1–2 years of age, $Na_V1.2$ in the distal part of the axon initial segment and the remaining axon is largely replaced by $Na_V1.6$, which takes over the process of AP initiation, whereas $Na_V1.2$ mainly contributes to back-propagation of APs to somatodendritic compartments (1,2,4,5). Moreover, there are two major splice isoforms of *SCN2A* that use mutually exclusive copies of the fifth coding exon in neonatal (5N) and adult (5A) brains. The 5N isoform is thought to reduce neuronal excitability, possibly having a seizure-protective role during early brain development (6). The 5A:5N ratio increases during human brain development, reaching a ratio of at least 4:1 in the mature neocortex (7,8).

Received: November 14, 2022. **Revised:** February 23, 2023. **Accepted:** March 19, 2023

Pathogenic heterozygous variants affecting *SCN2A* are among the most common causes of neurodevelopmental disorders. They cause a spectrum of clinical features including mild (benign) to severe (treatment refractory) epilepsy, as well as intellectual disability (ID)/autism without seizures (9–12). How this phenotypic spectrum emerges is still not fully understood. Based on patch-clamp electrophysiology in heterologous expression systems and mouse models, compartmental modeling and genotype–phenotype correlation in patients, it is proposed that opposing loss-of-function (LOF) versus gain-of-function (GOF) effects of different variants on channel function may cause ID/autism (without seizures) versus epilepsy, respectively (4,13,14).

Homozygous *Scn2a* knockout (*Scn2a*$^{-/-}$) is perinatally lethal in mice (15), but haploinsufficient (*Scn2a*$^{+/-}$) mice are viable and have been studied by different groups (15–17). Impaired excitability and excitatory synapse function in cortical (5) and hippocampal (16) neurons of *Scn2a*$^{+/-}$ mice have been observed, but reported neurobehavioral features are variable. They range from no significant abnormality (5) to impaired spatial learning (18,19) and reduced reactivity toward stressful stimuli (18), to absence-like seizures (20), likely depending on genetic background and experimental conditions.

CRISPR-generated *Scn2a*$^{\Delta 1898/+}$ mice display abnormal social interactions, accompanied by reduced neuronal excitability in culture and brain slices (21). On the other hand, mice harboring the GAL879-881QQQ or R1882Q mutation display neuronal hyperexcitability and have been used as epilepsy models (22–24).

Surprisingly, two recent studies demonstrated paradoxical hyperexcitability in prefrontal pyramidal and striatal principal neurons following complete or severe $Na_V1.2$ loss in postnatal mice (17,25). They provide evidence that $Na_V1.2$ deficiency can cause a reduction in the expression or function of potassium channels, which may prevent proper repolarization of neurons between APs and allow them to reach the threshold for subsequent APs more rapidly. In addition, certain *SCN2A* variants show mixed GOF and LOF effects in mouse models and heterologous systems (26,27). These findings highlight the complexity of neuronal sodium channel dynamics and the pathomechanisms of *SCN2A*-related disorders. Consequences of channel variants on neuronal function are thus difficult to predict, even with knowledge of how channel biophysics are altered. Human-based neuronal model systems may, therefore, be key to improve our understanding of how variants in channel genes affect neuronal function and cause distinct disease phenotypes.

Neurogenin-induced neurons derived from *SCN2A*$^{-/-}$ human-induced pluripotent stem cells (hiPSCs) (28) or *SCN2A*$^{+/-}$ embryonic stem cells (29) have been shown to display reduced spontaneous neuronal and network firing activities. However, electrophysiological properties of $Na_V1.2$ have not been studied in these mutant neurons.

The aim of this study was to explore the molecular and cellular effects of patient-specific *SCN2A* variants in a human-derived neurodevelopmental model with a focus on the less studied ID-causing variants. We therefore generated iPSC-derived neurons from patients with ID (without seizures) or EE harboring different *SCN2A* variants, and a CRISPR-Cas9-corrected isogenic line, and investigated them at the morphological, electrophysiological and transcriptomic levels compared with a neurotypical control at an early developmental stage (8 weeks in culture). Pathogenic ID variants consistently caused a reduction in $Na_V1.2$ protein level, neuronal sodium current density and AP firing. Neurons harboring a pathogenic epilepsy-causing variant displayed impaired sodium channel inactivation, but no obvious changes in AP firing. Single-cell transcriptomics identified dysregulated molecular pathways in patient-derived neurons including the inhibition of oxidative phosphorylation in ID neurons with *SCN2A* haploinsufficiency and activation of calcium signaling and neurotransmission in epilepsy neurons. Our results suggest that early-stage dysfunction of neuronal $Na_V1.2$ contributes to the etiology of *SCN2A*-related ID.

Results

Generation and characterization of patient and control iPSC-derived neurons

We generated iPSCs from dermal fibroblasts of four patients (Pts. 1–4) and a healthy control (Ctrl). Three patients (Pts. 1–3) were diagnosed with ID and autistic features but no seizures, and one patient with EE, all harboring de novo *SCN2A* (NM_021007.2) pathogenic variants (Fig. 1A, Supplementary Material, Table S1). Pt.1 had a frameshift variant [exon 12/27; p.(Leu611Valfs*35)] in the first intracellular linker domain, Pt.2 had a missense [exon 16/27; p.(Arg937Cys)] and Pt.3 a stop variant [exon 27/27; p.(Trp1716*)], both in the pore segments. Pt.4 (the EE patient) had a missense variant in the C-terminal [exon 27/27; p.(Glu1803Gly)]. An isogenic control line (iso-Ctrl) was generated by CRISPR-Cas9 editing (Supplementary Material, Fig. S1) of the variant in iPSCs of Pt.3. To generate neural progenitor cells (NPCs), we used iPSC lines that expressed NANOG, OCT3/4 and TRA-1-60 pluripotency markers (Supplementary Material, Fig. S2) in > 90% of the cells and harbored no newly occurring pathogenic copy number or sequence variants. NPC lines expressing Nestin and SOX2 (>90% of cells), and PAX6 (>80% of cells) (Supplementary Material, Fig. S3) were used for final neuronal differentiation.

Most of the cells in 8-week-old neuronal cultures expressed neuron-specific markers (e.g., MAP2, Supplementary Material, Figs S4 and S5), cortical layer-specific transcription factor CTIP2 (*BCL11B*, layer V) and vesicular glutamate transporter VGLUT2 (*SLC17A6*), confirming their cortical glutamatergic identity (Supplementary Material, Figs S4 and S5). A small fraction of cells expressed GABAergic markers (GABA and *GAD1/2*, Supplementary Material, Figs S4 and S5), which constituted < 12%. Markers of other neuronal subtypes or neural crest cells were scarcely expressed (Supplementary Material, Fig. S5). The astrocytic marker GFAP was variably expressed among different neuronal cultures (Supplementary Material, Figs S4 and S5).

Morphological assessment did not reveal major differences between patient- and control-derived neurons. The number of primary neurites, number of branching points, total neurite length and Sholl analysis of branching pattern were similar at four weeks (Supplementary Material, Fig. S6). However, neurons of Pt.4 (EE) had smaller somata than controls at four and eight weeks (adjusted $p = 0.01$ and $p = 2.0E^{-4}$, Supplementary Material, Fig. S6), suggesting a potentially delayed development of these neurons.

Variant-specific effects on *SCN2A*/$Na_V1.2$ expression

SCN2A mRNA and $Na_V1.2$ protein were clearly detectable in 8-week-old neurons (Fig. 1C–F). Furthermore, we detected both *SCN2A* mRNA isoforms (5A and 5N) in the neurons (5A:5N ratio ~ 1:2, Supplementary Material, Fig. S7).

Neuronal cultures from Pt.1 expressed significantly lower amounts of *SCN2A* mRNA and $Na_V1.2$ protein compared with the controls and other patients (Fig. 1D–F). This finding suggests nonsense-mediated decay of the aberrant allele and *SCN2A* haploinsufficiency in the neurons of Pt.1. 5A:5N ratio was also

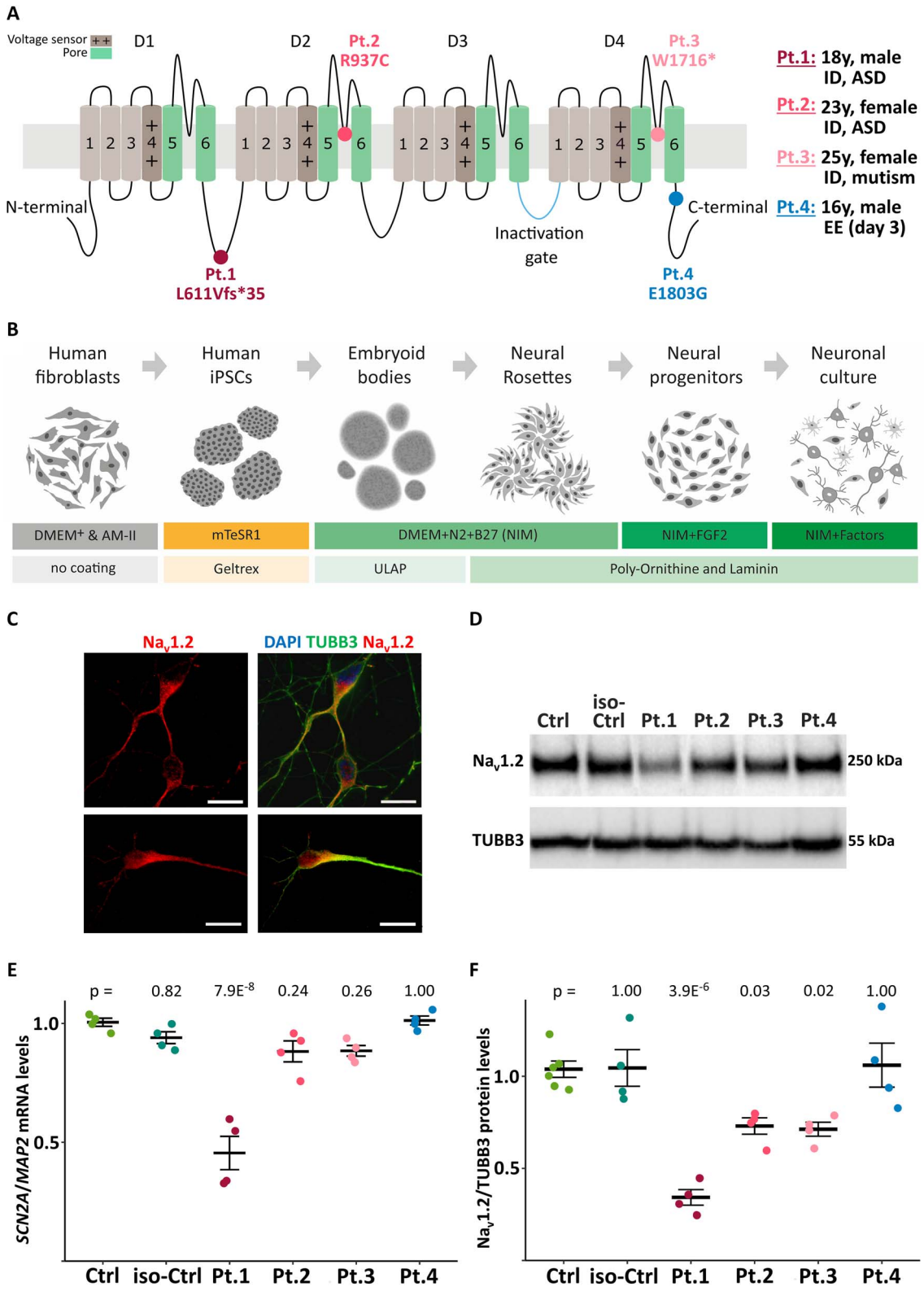

Figure 1. Effect of *SCN2A* pathogenic variants on *SCN2A*/$Na_V1.2$ expression can be assessed in hiPSC-derived neurons. (**A**) Schematic representation of $Na_V1.2$ channel including four repeat domains (D1–D4) each containing six membrane-spanning segments (S1–6). S4 acts as the channel's voltage sensor and S5–S6 create the channel's pore. Variants detected in our patients and their characteristics are shown on the right [p.(Leu611Valfs*35); p.(Arg937Cys); p.(Trp1716*); p.(Glu1803Gly)]. (**B**) Schematic overview of the protocol to generate hiPSC-derived neurons. Supplementary factors in the figure include ascorbic acid, cAMP, BDNF, GDNF and laminin (see Materials and Methods). (**C**) Immunofluorescence staining of our hiPSC-derived neurons suggesting the distribution of $Na_V1.2$ along the neurites and a polarized expression pattern near the soma. (**D**) $Na_V1.2$ protein expression in neuronal cultures of patients and controls shown by WB. (**E**) Quantitative RT-PCR, and (**F**) WB quantification showing a clear reduction of *SCN2A*/$Na_V1.2$ in neurons of Pt.1 harboring the frameshift variant, and WB revealing statistically significant reduction of $Na_V1.2$ in neurons of Pt.2 and Pt.3 compared with controls (two differentiations from two iPSC clones). Error bars represent SEM. AM-II, AmnioMAX-II; EE, epileptic encephalopathy; ID, intellectual disability; NIM, neural induction medium; Pt., patient; ULAP, ultra-low attachment plate; y, year.

significantly lower in neuronal cultures from Pt.1 compared with controls (Supplementary Material, Fig. S7b). In neuronal cultures from Pts. 2 and 3 harboring missense or stop variants, $Na_V1.2$ protein, but not the mRNA, was statistically significantly lower (Fig. 1D–F), indicating possible instability of the mutated proteins leading to a lower detectable amount. Neuronal cultures from Pt.4 (EE) expressed *SCN2A* mRNA and $Na_V1.2$ protein levels comparable with controls (Fig. 1D–F).

Differential effect of *SCN2A* variants on sodium current density and channel inactivation

Whole-cell patch-clamp recordings of early-stage (6 to 8 weeks old) human iPSC-derived control neurons revealed typical ionic currents, a hyperpolarized membrane potential and predominantly regular AP-firing (Supplementary Material, Fig. S8). Further electrophysiological assessments were performed in 8-week-old neurons because we observed a higher number of APs compared with 6-week-old neurons (Supplementary Material, Fig. S8f). We used voltage-clamp recordings to probe the impact of *SCN2A* variants on sodium currents in iPSC-derived neurons from controls and Pts. 1–4 (Fig. 2A–C). Voltage commands to membrane potentials between −80 and 60 mV caused inward- and outward currents in these neurons (Fig. 2C). We used the maximum peak inward current amplitude to calculate sodium current densities. Peak sodium current densities were significantly smaller in ID neurons (Pts. 1–3) compared with controls (Fig. 2D and E), consistent with lower $Na_V1.2$ protein levels. Intriguingly, the frameshift variant (Pt.1) caused a more pronounced reduction in maximum current density than the other two ID-causing variants (Cohen's $d = -1.15$ [95%CI −1.8; −0.73] vs. −0.47 [95%CI −0.9; 0.14] and −0.63 [95%CI −1.01; 0.02]). In contrast, sodium current density was comparable between EE neurons (Pt.4) and controls (Fig. 2D and E). Analysis of steady-state potassium currents revealed similar potassium current densities in neurons from patients and controls (Supplementary Material, Fig. S9a–c).

Based on our previous study showing an effect of the Glu1803Gly variant of Pt.4 (EE) on sodium channel inactivation in HEK cells (30), we next studied the voltage-dependence and gating kinetics of sodium channel inactivation in hiPSC-derived neurons. We recorded sodium currents after blocking voltage-gated potassium and calcium channels (see Materials and Methods). Inactivation time constants were obtained by fitting a monoexponential function to the decay of sodium currents at command voltages between −20 and 20 mV. We observed significantly longer inactivation time constants in EE, but not ID neurons (Fig. 2F and G; Cohen's $d = 1.28$ [95%CI 0.61; 1.81]), suggesting slower gating kinetics in EE neurons. Similar results were obtained by outside-out patch recordings without isolating sodium currents (Supplementary Material, Fig. S10a). In addition to gating kinetics, the voltage dependence of activation and inactivation is critical for sodium channel function. We probed sodium channel activation and inactivation kinetics in outside-out or nucleated patches excised from the soma of hiPSC-derived neurons. Analysis of midpoint potentials ($V_{1/2}$) revealed a significant depolarizing shift of steady-state inactivation in EE neurons (Fig. 2H and I; Cohen's $d = 1.86$ [95.0%CI 0.915; 2.87]). In ID neurons, there were no changes in voltage dependence of sodium channel activation or inactivation assessed by whole-cell recordings (Supplementary Material, Fig. S9d–f). Further analysis of sodium currents revealed indications for an enhanced persistent sodium current in Pt.4 (Supplementary Material, Fig. S10b; Cohen's $d = 1.18$ [95%CI 0.502; 1.79]), together with a slightly faster recovery from inactivation (Supplementary Material, Fig. S10c; Cohen's $d = -0.77$ [95.0%CI −1.37; −0.08]), whereas the onset of inactivation was not changed (Supplementary Material, Fig. S10d). The altered sodium channel inactivation characteristics in Pt.4 are in line with our previous data in HEK cells (30), underscoring the validity of a hiPSC-derived neuronal culture system to study ion channel variants on a cellular level.

Overall, ID-causing *SCN2A* variants led to reduced sodium current density in our patient-derived neurons, whereas the EE-causing Glu1803Gly variant specifically impaired sodium channel inactivation.

Reduced excitability in neurons harboring ID-causing *SCN2A* variants

The altered sodium current properties in patient-derived neurons harboring ID- and EE-causing *SCN2A* variants may influence neuronal excitability. We therefore performed current-clamp recordings to assess excitability, AP shape and passive membrane properties in hiPSC-derived neurons (Fig. 3A). We did not observe differences in membrane capacitance or resting membrane potential between patient- and control-derived neurons (Supplementary Material, Fig. S11a–b). Current injections to elicit AP firing revealed significantly fewer APs in ID neurons compared with controls (Fig. 3B), with a larger fraction of neurons that fired abortive or no APs (Fig. 3C). These data provide evidence that reduced $Na_V1.2$ levels or function impair AP firing in developing human neurons. In addition, evoked APs in Pt.1 and Pt.4 neurons had smaller amplitudes, whereas AP duration was not significantly altered (Supplementary Material, Fig. S11c–g). These data indicate that 8-week-old human neurons express functional $Na_V1.2$ channels that contribute to AP initiation and shape. Furthermore, our results demonstrate that ID-causing *SCN2A* variants reduce excitability in early-stage hiPSC-derived neurons. Intriguingly, despite changes in sodium channel inactivation (Fig. 2 and Supplementary Material, Fig. S10), AP properties and excitability of EE neurons (Pt.4) were largely like controls (Fig. 3C and D, Supplementary Material, Fig. S11).

Dimensionality reduction via Uniform Manifold Approximation and Projection (UMAP) followed by unsupervised clustering analysis of electrophysiological data recorded from hiPSC-derived neurons revealed that control cells and EE neurons separate from ID patient-derived neurons (Fig. 3E and Supplementary Material, Fig. S11h). This indicates that electrophysiological characterization can be employed to probe effects of *SCN2A*-variants on neuronal ion channel function and excitability.

To gain further insights into how *SCN2A* variants—in particular the Glu1803Gly variant of Pt.4—affect neuronal excitability and AP properties, we performed compartmental modeling.

In a model of a developing mouse cortical pyramidal neuron (13), we reduced $Na_V1.2$ conductance or incorporated the observed sodium channel gating differences to study patient-specific alterations of sodium channel function (Fig. 3F). Current injections produced repetitive AP firing in the wild-type model (100% *SCN2A*) but lowering $Na_V1.2$ conductance to 50 (50% *SCN2A*) or 0% (no *SCN2A*) strongly reduced AP firing in a dose-dependent manner (Fig. 3G). Incorporating the experimentally observed depolarizing shifts of sodium channel activation and inactivation by the Glu1803Gly variant of Pt.4 (2 and 10 mV, respectively, Fig. 2I), however, had little effect on AP firing. These findings are in line with our experimental results from Pt.4 neurons. Furthermore, reducing $Na_V1.2$ conductance caused strong decreases in AP firing across different levels of current injection (Fig. 3H), suggesting that lower $Na_V1.2$ levels reduce neuronal excitability. Together, compartmental modeling confirms

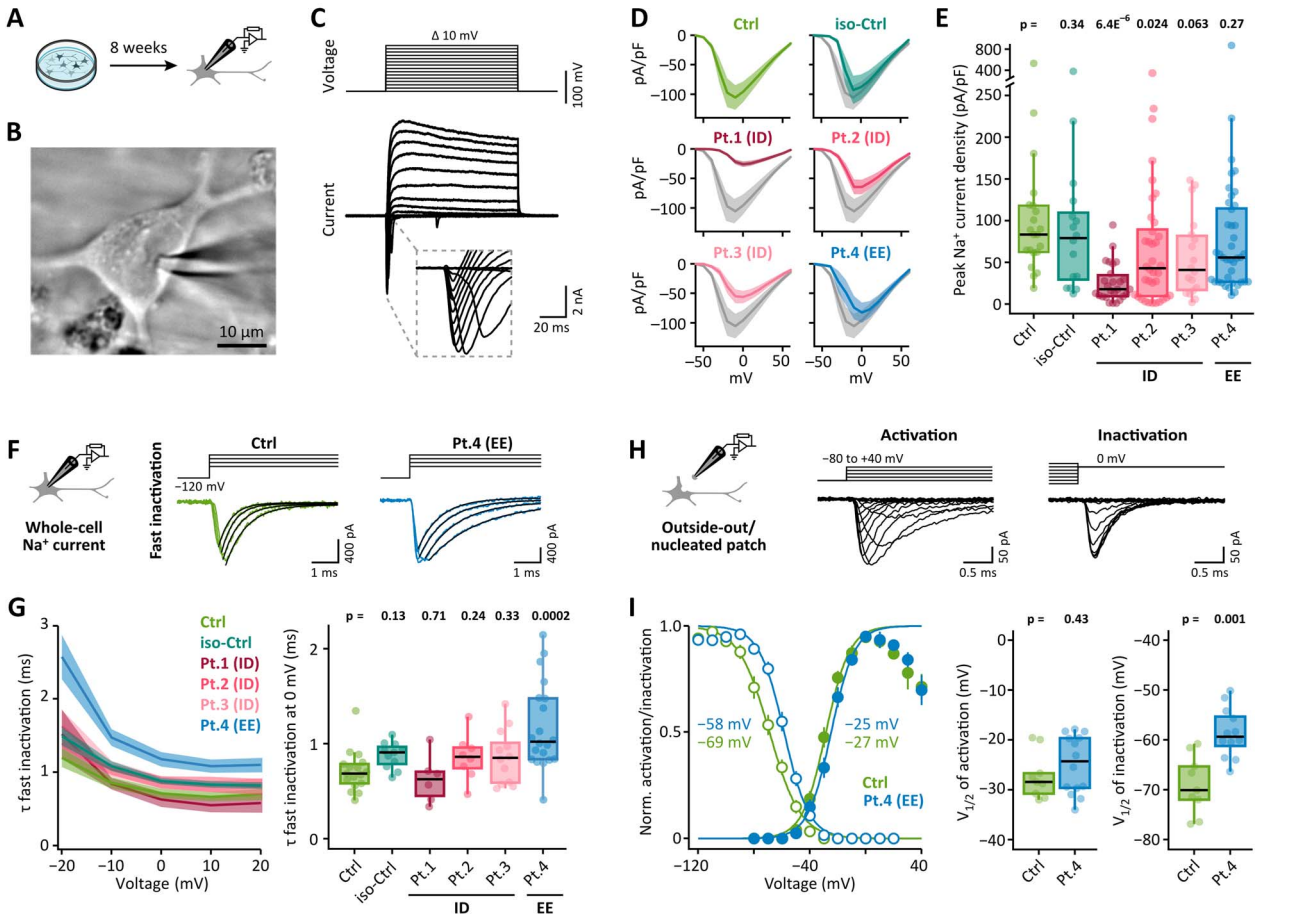

Figure 2. *SCN2A* pathogenic variants differentially affect sodium currents and channel gating in 8-week-old hiPSC-derived neurons. (**A**). Schematic of electrophysiological experiments. hiPSC-derived neurons were analyzed after 8 weeks in culture. (**B**) Example image of a neuron during patch-clamp recording. (**C**) Example whole-cell voltage-clamp recording. Top: voltage command. Bottom: whole-cell currents recorded from a representative neuron. Inset: inward currents on enlarged time scale. (**D**) Sodium current density versus voltage for Ctrl, iso-Ctrl and Pts. 1–4 (color-coded). Lines are means, and the shaded area represents SEM. For comparison, control data are replotted in gray in each graph. (**E**) Maximum sodium current density was significantly reduced in Pts. 1–3 with ID-causing *SCN2A* variants (Kruskal–Wallis: χ^2 (5) = 28.95, $p = 2.4E^{-5}$, $\eta^2 = 0.19$). Results of post hoc Dunn's test with Bonferroni–Holm correction are indicated. (**F**) Voltage protocol to study Na^+ channel fast inactivation and example currents from Ctrl and Pt.4. (**G**) Left: time constant of fast inactivation plotted versus voltage for controls and patients. Lines are means with shaded area representing ± SEM. Right: time constant of fast inactivation at 0 mV was increased in Pt.4 (Kruskal–Wallis: χ^2 (5) = 21.56, $p = 0.001$, $\eta^2 = 0.3$; results from post hoc Dunn's test with Bonferroni–Holm correction are indicated). (**H**) Top: voltage protocols to probe voltage-dependence of sodium current activation and inactivation in nucleated patches from neurons. Sodium currents were isolated by blocking voltage-gated potassium and calcium channels. Bottom: normalized activation and inactivation for control and Pt.4 versus voltage. Data are means with error bars denoting SEM; lines are sigmoidal fits, and midpoints values of activation and inactivation are indicated. (**I**) Left: midpoint ($V_{1/2}$) of activation was not significantly different between control and Pt.4. Right: $V_{1/2}$ of inactivation was significantly increased in Pt.4.

that reduced $Na_V1.2$ levels reduce AP firing and further indicates that the Glu1803Gly variant has only a moderate impact on AP firing under the studied conditions.

Our electrophysiological analyses of hiPSC-derived cortical neurons and computational modeling support the idea that ID-causing *SCN2A* variants decrease AP firing (i.e. neuronal excitability) and change AP shape in early-stage neurons by reducing sodium current density. At this developmental stage, the EE-causing Glu1803Gly variant primarily affects sodium channel inactivation without obvious effects on AP-firing and excitability.

Dysregulated pathways detected by single cell transcriptomics

Our single-cell RNA-seq data showed that cells in NPC cultures predominantly expressed neural progenitor (*NES*, *SOX2* and *PAX6*) and proliferation (*MKI67*) markers and cells in neuronal cultures mainly expressed neuronal (*MAP2*, Fig. 4A), glutamatergic (*SLC17A6/7*) and layer V cortical (*BCL11B*) markers (Supplementary Material, Fig. S5).

Remarkably, the most variably expressed genes in neurons of *SCN2A* patients, controls (isogenic and neurotypical) and a *KDM3B*$^{+/-}$ mutant line clustered separately (Fig. 4B, which was not the case for NPCs, Supplementary Material, Fig. S12), indicative of having distinct expression profiles upon differentiation.

Looking at differentially expressed genes (DEGs) in patients' and *KDM3B*$^{+/-}$ mutant neurons compared with controls, we found a large number of DEGs [mean (upregulated, downregulated)]: Pt.1: 1528 (850, 678), Pt.2: 1403 (709, 694), Pt.3: 1088 (449, 639), Pt.41245 (690, 555) and *KDM3B*$^{+/-}$ 2030 (919, 1111) (Fig. 5A and B). The mean of average log2-fold changes of DEGs were between +1.9 and −2.4, +2.5 and −3.1, +2.9 and −3.1, +2.1 and −3.0 and + 3.0 and −3.5, respectively. Supplementary Material, Table S2 lists the top 10 up- and downregulated DEGs.

Pathway analysis of all consistently detected DEGs by QIAGEN Ingenuity Pathway Analysis (IPA) software revealed similarly and

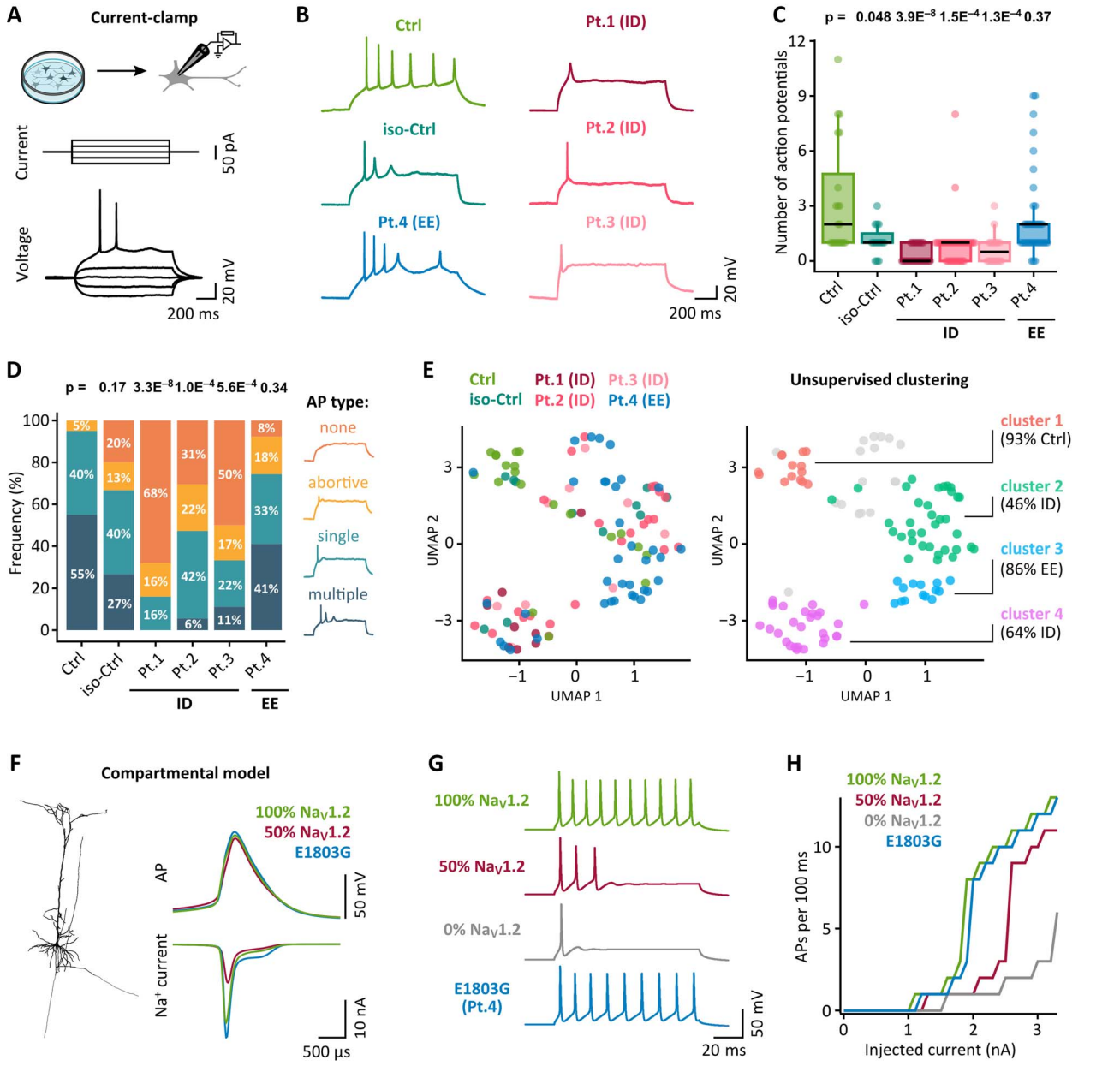

Figure 3. *SCN2A* pathogenic variants differentially affect action potential firing in 8-week-old hiPSC-derived neurons. (**A**) Top: schematic of recordings from hiPSC-derived neurons. Middle: step current injection protocol. Bottom: Example voltages recorded from a neuron in current-clamp mode. (**B**) Example voltage responses to positive current injections in different patient-derived neurons. (**C**) Neurons from patients with ID-causing *SCN2A* variants fired fewer APs (Kruskal–Wallis: $\chi^2(5) = 55.6$, $p = 9.84E^{-11}$, $\eta^2 = 0.37$). Results of post hoc Dunn's test with Bonferroni–Holm correction are indicated. (**D**) Neurons from ID patients displayed no or abortive AP firing more frequently than controls (Chi-square: $\chi^2(15) = 62.0$, $p = 1.14E^{-7}$, Cramer's $V = 0.32$). Results of post hoc Fisher's exact test with Bonferroni–Holm correction are indicated. (**E**) UMAP plot of electrophysiological data labeled for hiPSC line (left) or using HDBSCAN clustering result (right). Control cells and EE neurons tend to cluster separately from ID neurons. (**F**) Effects of *SCN2A* variants were studied in a mouse layer 5 pyramidal cell compartmental model (see Materials and Methods). Left: shape of the reconstructed neuron based on (46). Right: action potential as well as sodium current traces. (**G**) Membrane voltage in response to 2.2-nA current injections (duration, 100 ms) for different levels of $Na_V1.2$ conductance (100, 50 and 0%) and the Glu1803Gly variant (Pt.4 with a depolarizing shift of $Na_V1.2$ inactivation). (**H**) Number of APs per 100-ms current injection for different levels of $Na_V1.2$ conductance and Glu1803Gly. Reducing $Na_V1.2$ conductance decreases neuronal excitability, whereas the Glu1803Gly variant has little effect.

differently affected pathways among the mutant lines (Fig. 5C, Supplementary Material, Fig. S13). We detected two distinguishingly inhibited pathways, including the oxidative phosphorylation pathway (z-score −2.4) and the pathway of THOP1 neuroprotective role in Alzheimer's disease (z-score −2.2), in neurons of Pt.1 (ID), and one distinguishingly inhibited pathway: cholesterol biosynthesis (z-score −2.8), in neurons of Pt.3 (ID) (Fig. 5C, Supplementary Material, Tables S3 and S7). Intriguingly, three pathways were distinguishingly activated in Pt.4 (EE): synaptogenesis (z-score 5.1), synaptic long-term potentiation (LTP, z-score 3.4) and calcium signaling (z-score 3.3), all belonging to the category of neurotransmitter and second messenger signaling (Fig. 5C, Supplementary Material, Tables S3 and S7). WebGestalt gene set enrichment analysis also revealed transmission across chemical synapses (adjusted $p = 3.7E^{-4}$) and neurotransmitter release cycle (adjusted $p = 3.3E^{-4}$) as the top upregulated pathways in neurons

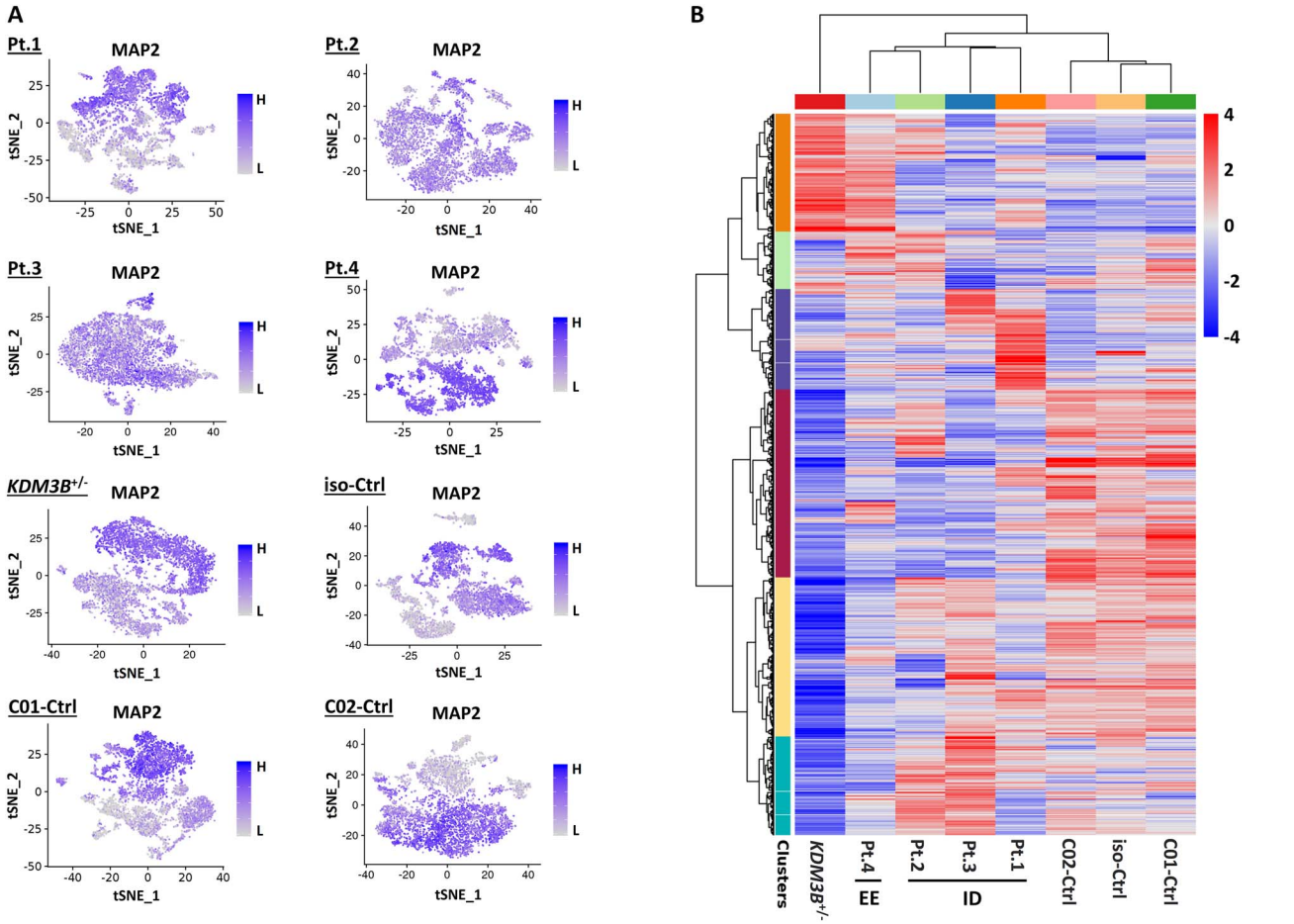

Figure 4. Expression profile of *MAP2*-positive cells in 8-week-old neuronal cultures discriminates between patients and controls. (**A**) t-SNE plot of *MAP2* expression in neuronal cultures from patients (Pts. 1–4, from one iPSC clone each), *KDM3B*$^{+/-}$ mutant (from one iPSC clone), isogenic line and controls (Ctrl from two iPSC clones, C01 and C02). Each dot represents a cell in the neuronal culture, and shades of color correspond to the expression level of the neuronal marker, *MAP2*, present in 65–85% of the cells showing the predominant cell type in the neuronal cultures. (**B**) Pseudobulk heatmap of the most variable 2000 genes in the *MAP2*-positive cells of neuronal cultures from patients and controls. Threshold for standard deviation of log2 signal across samples was 1.09. Discriminative clustering of *SCN2A* patients, controls and *KDM3B*$^{+/-}$ mutant samples is evident.

of Pt.4. These findings may indicate a dysfunction of synaptic transmission in EE neurons of Pt.4.

We also detected the inhibition of JAK/Stat (z-score −2.2) and activation of sumoylation (z-score 2.1) as distinguishingly affected pathways (Fig. 5C, Supplementary Material, Tables S3 and S7) in the *KDM3B*$^{+/-}$ mutant neurons. Additional data would be available upon request.

Discussion

We studied the effects of pathogenic *SCN2A* variants causing ID without seizures or EE in hiPSC-derived early-stage neurons at multiple levels. Our data revealed the effects of variants on neuronal *SCN2A* mRNA and $Na_V1.2$ protein expression, sodium channel function, neuronal excitability and molecular signaling pathways. Our results provide further insights into the pathomechanisms of *SCN2A*-related disorders and demonstrate the value of hiPSC-based disease modeling.

Several *SCN2A* variants have been previously characterized by heterologous expression in non-neuronal cells revealing distinct alterations of $Na_V1.2$ channel biophysics (13,30). We previously investigated the same four *SCN2A* pathogenic variants in a heterologous expression system (30), and here demonstrate that the observed alterations of channel properties consistently translate into a patient-derived neuronal model. Sodium channel dysfunctions, including reduced current density by ID-causing variants and impaired inactivation by an EE-causing variant, occur at a relatively early developmental stage in hiPSC-derived neurons from patients. This is in line with previous studies detecting no measurable currents in non-neuronal cells transiently transfected with mutant cDNA of ID-causing variants (4,13,30). Intriguingly, we did not observe indications for compensations by other sodium channels or reductions in potassium currents. Consistent with the reduced sodium current density, $Na_V1.2$ protein levels were reduced in all ID neurons harboring frameshift, missense or stop variants. Because of smaller sodium currents, ID neurons fired fewer APs that also had an increased threshold and a reduced amplitude. Remarkably, neurons harboring the *SCN2A* frameshift variant expressed $Na_V1.2$ to a haploinsufficiency level, which also correlated with a more pronounced reduction in sodium current density and AP firing compared with the other variants. In contrast to the ID-causing variants, we detected no significant change in $Na_V1.2$ protein level or sodium current density in epilepsy neurons harboring the Glu1803Gly variant. Together, our results reveal that ID-causing *SCN2A* variants reduce neuronal $Na_V1.2$ expression, AP firing and excitability at early stages of neuronal development. As embryonic brain development is largely dependent on neuronal electrical activity (31,32), our data

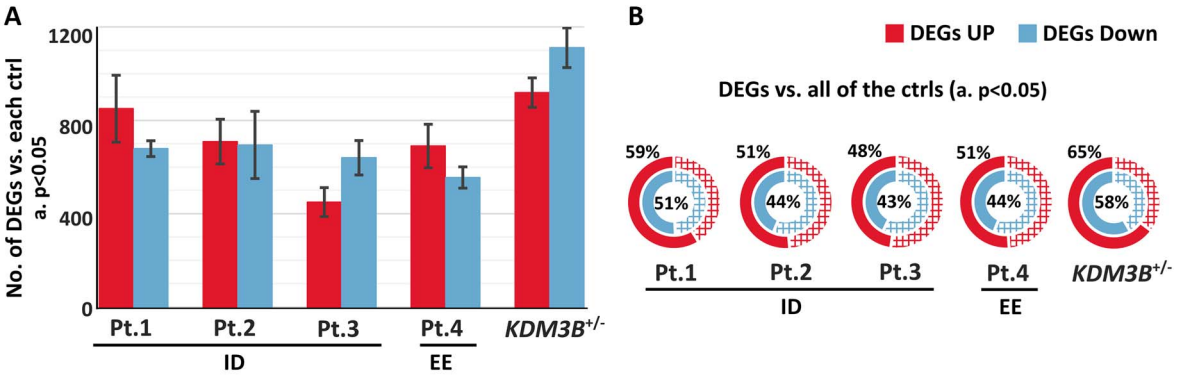

C

Canonical signaling pathway	Pt.1 (ID)	Pt.2 (ID)	Pt.3 (ID)	Pt.4 (EE)	*KDM3B* $^{+/-}$
Glycoprotein VI (GP6)	-2.1	-3.4	-2.6	-1.9	-3.3
Unfolded protein response	-0.7	-2.8	-0.4	-1.7	-2.5
STAT3	-0.6	-2.1	-2.1	-1.5	-2.7
PI3K/AKT	-0.4	-2.2	-1.5	-0.6	-1.0
G alpha (i)	-1.3	-2.1	-1.6	-0.7	-1.7
Synaptogenesis*	0.9	0.0	0.6	5.1	0.3
Glycolysis I	2.3	2.2	0.9	0.8	1.3
PPAR	0.8	1.9	2.8	0.6	3.1
Neurotrophin/TRK	2.2	0.8	0.2	2.8	0.3
PPAR-alpha/RXR-alpha activation	0.2	2.1	0.7	1.0	1.0
Oxidative phosphorylation*	-2.4	0.8	1.8	2.1	0.9
Neuroprotective role of THOP1 in AD*	-2.2	0.0	0.0	0.2	0.0
BAG2	1.4	-1.9	-0.4	-1.0	-2.6
Cholesterol biosynthesis*	0.3	0.2	-2.8	0.0	1.2
EIF2	3.4	1.0	3.1	-2.3	3.7
RhoGDI	0.9	0.6	0.9	-1.2	2.0
Synaptic LTP*	-1.3	-0.6	-0.9	3.4	-0.9
Calcium*	-2.3	-0.4	-1.1	3.3	0.2
Ephrin receptor	-1.7	-0.2	-2.7	2.7	-1.0
G beta gamma	-0.3	-1.0	-1.4	2.5	-0.2
Integrin	-0.2	-0.2	-2.2	2.3	-1.5
ERK5	0.0	-1.4	-1.3	2.3	-0.3
G alpha q	-0.6	0.0	-0.7	2.3	-1.9
Phospholipase C	-0.4	-0.6	-1.7	2.2	-1.3
Actin cytoskeleton	-0.2	-1.3	-2.2	2.1	-1.5
Rho family GTPases	-0.8	-0.2	-2.2	2.0	-3.0
Huntington's disease	-0.6	-1.2	-0.2	2.0	0.2
Actin nucleation by ARP-WASP complex	-2.2	-0.6	-2.4	1.6	-2.1
Regulation of actin-based motility by Rho	-1.7	-0.9	-2.9	1.4	-1.1
CREB in neurons	-0.8	-2.7	-1.6	1.3	-2.7
Synaptic LTD	-0.7	-2.3	-1.3	1.3	-1.7
JAK/Stat*	0.8	0.4	0.0	1.6	-2.2
Relaxin	1.5	0.2	0.7	2.8	-1.7
eNOS	1.4	0.6	0.8	2.2	-0.8
EGF	2.0	1.0	0.3	1.9	-0.3
P2Y purigenic receptor	2.1	0.2	0.4	2.9	-0.2
Sumoylation*	-0.4	0.2	0.3	0.3	2.1
3-phosphoinositide biosynthesis	2.3	-0.4	-1.3	2.0	1.3
3-phosphoinositide degradation	1.3	-0.4	-1.3	1.8	1.1
Reelin in neurons	1.8	-1.0	-1.3	1.6	-0.7
Neuregulin	2.4	-1.0	-1.0	0.6	0.5
GDNF family ligand-receptor interactions	0.8	0.4	-1.0	2.1	-0.6
HIF1-alpha	2.1	-0.4	-0.7	0.3	-1.4

Figure 5. Significant differentially expressed genes (DEGs) render to distinguishing signaling pathways (activated and inhibited) in mutant hiPSC-derived neurons. (**A**) Number of DEGs versus each control (error bars represent SEM) and (**B**) percentage of DEGs consistently observed versus all controls (see Materials and Methods) with adjusted (a) *P*-value < 0.05 in neurons of *SCN2A*-patients and the *KDM3B*$^{+/-}$ mutant. (**C**) Heatmap table of significantly affected pathways (inhibited or activated) in neurons of Pts. 1–4 and the *KDM3B*$^{+/-}$ mutant, and the corresponding z-score calculated by IPA. Notably, synaptogenesis, calcium and synaptic LTP signaling pathways were specifically activated in epilepsy patient neurons.

further support the hypothesis that *SCN2A* variants with LOF effects may cause ID by reducing sodium currents and excitability (13,15,16,18,21).

Epilepsy-causing *SCN2A* variants are generally thought to exert GOF effects and promote neuronal excitability (13,22,23). Consistent with this idea, we observed impaired sodium channel inactivation and a prolonged decay of sodium currents in epilepsy neurons harboring the Glu1803Gly variant in the C-terminal domain. This finding is in agreement with our previous results from heterologous expression in HEK cells and structural modeling that predicted a disturbance of contacts between the C-terminal domain and the inactivation gate (30). These findings suggest that a change in sodium channel inactivation may contribute to the epilepsy phenotype caused by this variant. Intriguingly, several other epilepsy-causing *SCN2A* variants have been shown to impair $Na_V1.2$ inactivation or enhance persistent sodium currents (11,30,33). Slower sodium channel inactivation kinetics may prolong AP duration. Although the median AP duration of EE patient-derived neurons was longer than in controls (3.8 ms vs. 2.8 ms), the broad data distributions did not allow resolving potential differences.

Furthermore, a depolarizing shift in the voltage dependence of fast inactivation and slower inactivation kinetics would be expected to increase sodium influx during an AP and promote repetitive AP firing. However, we did not observe major differences in the number or properties of APs in early-stage neurons from the EE-patient studied here. Whether hyperexcitability at the level of AP firing occurs at later developmental stages requires further investigation of more mature iPSC-derived neurons. Nevertheless, it is striking that our transcriptome analyses revealed the activation of neurotransmitter- and second messenger-related signaling, particularly synaptogenesis, synaptic LTP and calcium signaling pathways specifically in epilepsy neurons. These data suggest a possible hyperactivity state in epilepsy neurons at the molecular level converging onto synaptic transmission pathways, which may point towards the following possible hypotheses. As $Na_V1.2$ was recently shown to be calcium-permeable (34), impaired $Na_V1.2$ inactivation may increase calcium influx and thereby promote calcium signaling and neurotransmission in epilepsy neurons. Alternatively, increased sodium influx might activate the Na^+/Ca^{2+} exchanger, potentially increasing net intracellular calcium concentration and facilitating neurotransmitter release at synapses (35). Considering the recent data on paradoxical hyperexcitability following complete or severe $Na_V1.2$ loss in postnatal mice (17,25) and a relative increase in the number of APs in hiPSC-derived neurons harboring another EE-causing variant (Leu1342Pro) (36), it is conceivable that different EE-causing *SCN2A* variants have distinct effects. Investigation of additional patients is required to determine the spectrum of excitability changes caused by different epilepsy-causing variants.

Moreover, we also observed altered signaling pathways in the ID neurons. Neurons harboring the frameshift variant with $Na_V1.2$ haploinsufficiency displayed inhibition of the oxidative phosphorylation pathway. Oxidative phosphorylation generates ATP in mitochondria and is fundamental for neurogenesis, brain development and neuronal function (37,38). It has also been previously linked to neurodevelopmental and neurodegenerative disorders (38). We did not detect this pathway to be similarly affected in the ID neurons harboring the other two variants, which may suggest specificity for *SCN2A* haploinsufficiency. Furthermore, there were distinctively affected pathways in *KDM3B*$^{+/-}$ neurons used as an independent mutant line in this study. Since *KDM3B* pathogenic variants also cause ID (39), our data imply the specificity of the transcriptome and pathway profiles in hiPSC-derived neurons depending on the affected gene and variant type. Detected transcriptome signatures may reflect a homeostatic response of neurons to $Na_V1.2$ dysfunction, which can guide further investigations into the pathophysiology and treatment of *SCN2A*-related disorders.

In this study, age, gender and genetic background were not controlled as we compared patient-derived lines with lines from a young healthy female control. However, two of the ID patients were females with similar age to the control. In addition, our sodium current recordings capture characteristics of all sodium channels expressed in the generated neurons and are therefore not specific for $Na_V1.2$. Nevertheless, we consistently observed reduced $Na_V1.2$ levels in ID neurons, which is likely the main reason for the reduced sodium current density in these neurons, independent of other sodium channels. These limitations should be considered when interpreting the data, especially in the case of the epilepsy neurons that were derived from only one patient.

In conclusion, our study revealed discriminative electrophysiological signatures between ID- and epilepsy-causing *SCN2A* variants and controls in early-stage iPSC-derived neurons. We also showed differentially affected transcriptional pathways in neurons harboring the *SCN2A* frameshift variant causing ID and the *SCN2A* missense variant causing EE. Our data further support the LOF effect of ID-causing variants by a significant reduction in neuronal $Na_V1.2$ protein levels, sodium current density and AP firing. The pathomechanisms of epilepsy-causing variants, on the other hand, appear to be more complex. Patient iPSC-derived neurons provide a valuable tool to investigate how *SCN2A* variants cause a diverse spectrum of neurodevelopmental disorders. They provide the possibility to study patient-specific variants in a heterozygous state and in human neuronal cells thus paving the way for precision medicine approaches.

Materials and Methods

Participants and fibroblast derivation

Three patients with ID but no seizures (Pts. 1–3) and one patient with EE (Pt.4), all previously published with de novo *SCN2A* pathogenic variants (30) (Fig. 1A) and a neurotypical female control were included in this study (Supplementary Material, Table S1). Standard skin-punch biopsies from the participants were cultured according to standard protocols (Supplementary Methods). Fibroblast samples were analyzed for genomic stability before reprogramming. This study was part of a research program approved by the ethics commission of the Canton of Zurich (StV 11/09 and PB_2016-02520). All individuals and/or their guardians signed informed consent.

Generation of hiPSCs

Low passage fibroblasts from patients and the control were reprogrammed into hiPSCs using CytoTune®-iPS 2.0 Sendai Reprogramming Kit (Invitrogen) according to the manufacturer's instructions. We generated multiple hiPSC lines from each individual and performed morphological and pluripotency marker (NANOG, OCT3/4, TRA-1-60) assessment, verification of genomic stability and regular mycoplasma testing as quality control measures. The hiPSCs were cultured in mTeSR™1 (STEMCELL Technologies) and 1% penicillin/streptomycin. Two quality-controlled hiPSC clones from each patient, the control (C01-Ctrl and C02-Ctrl) and a CRISPR-Cas9 edited line from Pt.3 (iso-Ctrl) were used for further assays.

Genomic stability analyses in fibroblasts and hiPSCs

Fibroblast and hiPSC lines used in this study were assessed to rule out newly acquired pathogenic chromosomal aberrations, copy number variants and sequence variants by conventional karyotyping, chromosomal microarray analysis (CMA) and whole exome sequencing (WES), respectively, as previously described (40). Samples harboring any new pathogenic genetic variant were excluded. An initial control hiPSC line which had acquired a pathogenic stop variant in *KDM3B* (NM_016604.3, c.4912C > T, p.(Gln1638*), exon 22/24) was further used as an independent mutant (*KDM3B*$^{+/-}$) in transcriptome analysis.

Flow cytometry

For quantitative measurement of pluripotency marker expression, hiPSC lines were stained by TRA-1-60 Alexa Fluor 488 conjugate and IgM isotype-matched Alexa Fluor 488 control (both Biolegend). A total of 10^5 cells were washed and stained in flow cytometry buffer (PBS, 2% FCS, 0.1% NaN3), and cells were assayed using a BD LSR II Fortessa. Data from 10 000 cells were collected and analyzed using FlowJo software, gated on FSC-SSC dot plots and plotted as histograms (y-axis normalized to mode).

CRISPR-Cas9-mediated genome editing

The hiPSC editing pipeline used is summarized in Supplementary Material, Fig. S1 and Table S4. Clones from Pt.3 with complete repair (no *SCN2A* variant in > 500 reads in WES) and no other pathogenic variant comprehensively evaluated by CMA and WES were used as an isogenic control (iso-Ctrl) for subsequent assays. Notably, this isogenic line was only considered as an independent control, all the experimental data from this isogenic line and the patients are compared with the control line. Experimental data of the patients are not compared with this isogenic line.

Differentiation of hiPSCs to neural progenitors and cortical neurons

hiPSCs were differentiated to NPCs and cortical neurons according to a previously published embryoid body (EB)-based protocol (41) with minor modifications (Fig. 1B, and Supplementary Methods). NPC lines of passage 5–7, which were positive for Nestin and SOX2 (>90%), and PAX6 (>80%) markers in immunocytochemistry were used for neuronal differentiation. Four- or eight-week-old neurons were used for different assays.

Immunocytochemistry

Cells were fixed in 4% paraformaldehyde for 15 min at room temperature and subsequently blocked and permeabilized in PBS containing 0.3% Triton X-100 and 3% donkey serum. Coverslips were incubated with primary antibodies (all listed in Supplementary Material, Table S5) in blocking solution overnight at 4°C and with secondary antibodies for 1 h at room temperature. Fluorescence signals were detected using Zeiss AxioPlan 2 or Zeiss AxioObserver Z1 microscopes, and images were processed with ZEISS ZEN lite and ImageJ software.

RT/qPCR

For targeted transcriptional analyses, RNA was extracted from cells using RNeasy Plus Mini Kit 50 (QIAGEN). Reverse transcription was performed using SuperScript III First-Strand Synthesis System (Invitrogen). RT-PCR was performed by PCR amplification of cDNA using specific primers (Supplementary Material, Table S4) and running the products on 1–1.5% agarose gel. qPCR was performed by PCR amplification of cDNA using specific primers (Supplementary Material, Table S6) and SYBR green (Roche) on a Roche LightCycler480. For quantification, *SCN2A* expression levels were normalized to *MAP2* levels.

Western blot

Cells were lysed as detailed in Supplementary Methods, and protein concentration was determined by bicinchoninic acid assay (Pierce BCA kit, Thermo Scientific). For detecting $Na_V1.2$, 10-μg protein samples were boiled (2 min, 90°C) in NuPAGE LDS Sample Buffer (Invitrogen, NP0007) and Sample Reducing Agent (Invitrogen, NP0004) and run in NuPAGE 3 to 8%, Tris-Acetate Gel (Invitrogen, EA0378BOX). Details of blotting, antibody incubation and signal detection are available in Supplementary Material, Table S5. Relative $Na_V1.2$ protein levels (ratio between $Na_V1.2$ and TUBB3 band density) were quantified using Image Lab 6.1 software (BioRad).

Neurite tracing, soma measurement and complexity analysis

Four-week-old neuronal cultures were transfected with pEF1-dTomato plasmid using Lipofectamine LTX (Invitrogen, transfection reagent/DNA 2:1) to visualize single cells (sparse labeling). 24 h post-transfection, cells were fixed with 4% paraformaldehyde and stained with anti-TUBB3 (Supplementary Material, Table S3). Images were captured using the TILE function of the Zen Pro Software on the AxioObserver Z1 fluorescence microscope (Zeiss). Semi-automated tracing of individual transfected neurons, outlining somata and Sholl analysis were performed using Fiji.

Electrophysiology

Eight weeks after induction, coverslips containing hiPSC-derived neurons were placed in a recording chamber mounted on an upright Scientifica SliceScope 2000 equipped with differential interference contrast (DIC) and a 60× objective. Whole-cell patch-clamp recordings were made from visually identified neurons. Recording pipettes (~5 MΩ) were pulled from borosilicate glass (Science Products) using a DMZ Puller (Zeitz Instruments). Pipettes contained (in mM): 150 K-gluconate, 10 NaCl, 10 HEPES, 3 MgATP, 0.3 NaGTP, 0.05 EGTA and pH adjusted to 7.3 using KOH. Voltages were corrected for a liquid junction potential of +13 mV. The bath solution contained (in mM): 135 NaCl, 10 HEPES, 10 glucose, 5 KCl, 2 $CaCl_2$ and 1 $MgCl_2$. Recordings were done using a HEKA EPC10 amplifier (HEKA Elektronik GmbH, Germany). For whole-cell voltage-clamp recordings, holding potential was −80 mV. Data were filtered at 10 kHz and digitized with 100–200 kHz. Series resistance was compensated online by 60–80% with a 10-μs delay. Cells with remaining series resistance > 10 MΩ were not included in the analysis. Voltage steps (duration, 100 ms) were applied from −80 mV to voltages between −80 and + 60 mV to study whole-cell currents. Leak and capacitance currents were subtracted using the P/4 method. Peak inward and outward currents were quantified and normalized to whole-cell capacitance. To study Na^+ channel activation and inactivation, recordings of Na^+ currents were performed by blocking voltage-gated K^+ and Ca^{2+} channels using a bath solution containing (in mM): 110 NaCl, 20 TEA-Cl, 10 HEPES, 10 glucose, 5 KCl, 5 4-AP, 2 $CaCl_2$, 1 $MgCl_2$, 0.1 $CdCl_2$ and an intracellular solution containing (in mM): 135 Cs-gluconate, 20 TEA-Cl, 10 HEPES, 5 Na_2-phosphocreatine, 4 MgATP, 0.3 NaGTP and 0.2 EGTA (pH adjusted to 7.3 using CsOH; voltages were corrected for a liquid junction potential of +13 mV). This Na^+ current isolation approach

captures features of all Na^+ channels expressed in the iPSC-derived neurons. For a subset of experiments, we isolated somatic outside-out or nucleated patches after obtaining the whole-cell configuration by slowly retracting the pipette while applying slight negative pressure (42). Voltage protocols to study Na^+ currents were similar to ref. (43). Peak activation and steady-state inactivation data were fit with a Boltzmann equation as described previously (43). We used current-clamp recordings to examine AP firing and membrane properties. Resting membrane potential was measured without current injection. Subsequently, current injection protocols (duration, 1 s; step, ±10 pA) were applied from a holding voltage of ~ − 80 mV. Current-clamp data were filtered at 2.7 kHz and digitized with 100 kHz. Experiments were performed at room temperature (21–25°C). All data were analyzed with custom-written routines in Igor Pro 6.3 software (WaveMetrics).

Computational modeling

Simulations were performed using the pyramidal cell model from Ben-Shalom et al. (13) and run in NEURON version 8.0 and Python version 3.8. The simulation time step was 20 μs. To study the effect of *SCN2A* mutations on neuronal excitability, Na_V channel distribution in the soma and axon initial segment represented the 'developing model' (13). Total g_{Na} was split into two instances of $Na_V1.2$/*SCN2A*. To model nonconducting variants, conductance of one (50% $Na_V1.2$) or both (0% $Na_V1.2$) $Na_V1.2$ instances was set to 0. To model the E1803G mutation, activation and inactivation of $Na_V1.2$ instances were shifted by 2 and 10 mV, respectively. Changes in $Na_V1.2$ properties reflecting patient variants were restricted to the axon initial segment of the model cell. The model and supporting files are available at https://github.com/delvendahl/SCN2A_simulations.

Single-cell (sc)RNA-seq using 10x genomics

To determine the cellular composition of NPCs (passages 5–7) and neuronal (8-week-old) cultures, and neuron-specific dysregulated pathways caused by *SCN2A* variants, we performed scRNA-seq of the cultures from patients and controls using 10x Genomics technology.

Cell preparation steps are summarized in Supplementary Methods. Cells were loaded onto a 10x Genomics Chromium platform targeting ~6000 cells per sample. Libraries were prepared with a Chromium Single Cell 3' Reagent Kit (v3.1) according to the manufacturer's instructions and were sequenced on an Illumina NovaSeq 6000 system in paired-end configuration targeting ~60 000 reads per cell. Our bioinformatics pipeline is summarized in Supplementary Methods.

To visualize cells in a low-dimensional space, t-distributed stochastic neighbor embedding of the principal components (t-SNE) was used as implemented in Seurat (44). Heatmaps of the most variable 2000 genes were generated by integrating multiple samples using the *cellranger aggr* command in Cell Ranger with normalization mode *mapped*. Counts from all cells in each sample were summed to produce a pseudobulk matrix.

To calculate DEGs, *NES*-positive and *MAP2*-negative cells of NPC cultures (NPCs) and *MAP2*-positive cells of neuronal cultures (neurons) in each patient versus each control (C01-Ctrl, C02-Ctrl and iso-Ctrl) were compared using *FindMarkers()* in Seurat (Wilcox test, logFC threshold = 0.25, minimum pct = 0.1). For each patient, DEGs with Bonferroni adjusted *P*-value < 0.05, which were consistently detected versus all controls, were used for further analysis.

Pathway analysis

DEGs and their average log2FC values were uploaded into the QIAGEN IPA software (version 62 089 861, Ingenuity Systems). Activation or inhibition of affected canonical pathways was measured by IPA activation z-score, which is a statistical measure of the match between expected relationship direction and observed gene expression (45). More activated than inhibited predictions result in $z > 0$ and vice versa predictions lead to $z < 0$. Pathways specifically annotating non-neuronal organ systems, or those with z-score smaller than ±2, were excluded. All other pathways in Pts. 1–4 and the $KDM3B^{+/-}$ independent mutant were considered. Pathways that were a) significantly dysregulated in neurons of a patient but not similarly in other patients and b) not affected in NPCs of the same patient were considered as distinguishingly affected pathways in neurons.

In addition, gene set enrichment analysis based on the Reactome database was performed for DEGs from neurons by WebGestalt (http://www.webgestalt.org/).

Statistical analyses

Data are presented as median values with boxes representing first and third quartiles. *N* refers to the total number of observations (cells) per experimental group. Statistical analysis was performed using R or SPSS software. For qPCR and western blot experiments, biological replicates were compared using one-way ANOVA and Tukey's post hoc test for multiple comparisons. Electrophysiological data were analyzed via Kruskal–Wallis H tests with an alpha level of 0.05, followed by post hoc Dunn's tests with Bonferroni–Holm correction. Post hoc tests compared non-control lines to control only. All *P*-values stated are adjusted for multiple comparisons, if applicable. Effect sizes are given as eta-squared for Kruskal–Wallis tests or Cohen's *d* for two group comparisons, respectively. Confidence intervals of effect sizes were obtained using bootstrap resampling with 5000 samples.

Acknowledgements

We thank all involved families for their participation and permission to publish the results. We would also like to thank Dr Jürg Böni, Dr Michael Huber and their team from the Institute of Medical Virology, University of Zurich, for performing virology testing of our samples.

Supplementary Material

Supplementary Material is available at *HMG* online.

Conflict of Interest statement. None declared.

Funding

Swiss National Science Foundation (320020_179547 to A.R.; PZ00P3_174018 to I.D.); University of Zurich Clinical Research Priority Program (Praeclare to A.R. and M.M.); University Research Priority Program of the University of Zurich (ITINERARE to A.R.); European Research Council Starting Grant (SynDegrade-679881 to M.M.); Bavarian Ministry of Education and Culture, Science and the Arts within the framework of the Bavarian Network for studying brain cell interactions (ForInter to B.W. and J.W.).

References

1. Hu, W., Tian, C., Li, T., Yang, M., Hou, H. and Shu, Y. (2009) Distinct contributions of $Na_v1.6$ and $Na_v1.2$ in action potential initiation and backpropagation. *Nat. Neurosci.*, **12**, 996–1002.
2. Martínez-Hernández, J., Ballesteros-Merino, C., Fernández-Alacid, L., Nicolau, J.C., Aguado, C. and Luján, R. (2013) Polarised localisation of the voltage-gated Sodium Channel $Na_v1.2$ in cerebellar granule cells. *Cerebellum*, **12**, 16–26.
3. Vacher, H., Mohapatra, D.P. and Trimmer, J.S. (2008) Localization and targeting of voltage-dependent ion channels in mammalian central neurons. *Physiol. Rev.*, **88**, 1407–1447.
4. Sanders, S.J., Campbell, A.J., Cottrell, J.R., Moller, R.S., Wagner, F.F., Auldridge, A.L., Bernier, R.A., Catterall, W.A., Chung, W.K., Empfield, J.R. *et al.* (2018) Progress in understanding and treating SCN2A-mediated disorders. *Trends Neurosci.*, **41**, 442–456.
5. Spratt, P.W.E., Ben-Shalom, R., Keeshen, C.M., Burke, K.J., Clarkson, R.L., Sanders, S.J. and Bender, K.J. (2019) The autism-associated gene Scn2a contributes to dendritic excitability and synaptic function in the prefrontal cortex. *Neuron*, **103**, 673–685.e5.
6. Gazina, E.V., Leaw, B.T.W., Richards, K.L., Wimmer, V.C., Kim, T.H., Aumann, T.D., Featherby, T.J., Churilov, L., Hammond, V.E., Reid, C.A. *et al.* (2015) 'Neonatal' $Na_v1.2$ reduces neuronal excitability and affects seizure susceptibility and behaviour. *Hum. Mol. Genet.*, **24**, 1457–1468.
7. Kasai, N., Fukushima, K., Ueki, Y., Prasad, S., Nosakowski, J., Sugata, K., Sugata, A., Nishizaki, K., Meyer, N.C. and Smith, R.J.H. (2001) Genomic structures of SCN2A and SCN3A – candidate genes for deafness at the DFNA16 locus. *Gene*, **264**, 113–122.
8. Liang, L., Fazel Darbandi, S., Pochareddy, S., Gulden, F.O., Gilson, M.C., Sheppard, B.K., Sahagun, A., An, J.-Y., Werling, D.M., Rubenstein, J.L.R. *et al.* (2021) Developmental dynamics of voltage-gated sodium channel isoform expression in the human and mouse brain. *Genome Med.*, **13**, 135.
9. Rauch, A., Wieczorek, D., Graf, E., Wieland, T., Endele, S., Schwarzmayr, T., Albrecht, B., Bartholdi, D., Beygo, J., Di Donato, N. *et al.* (2012) Range of genetic mutations associated with severe non-syndromic sporadic intellectual disability: an exome sequencing study. *Lancet*, **380**, 1674–1682.
10. Clayton, J.F., Fitzgerald, S., Kaplanis, T.W., Prigmore, J., Rajan, E., Sifrim, D., Aitken, S., A., Akawi, N., Alvi, M. *et al.* (2017) Prevalence and architecture of de novo mutations in developmental disorders. *Nature*, **542**, 433–438.
11. Wolff, M., Johannesen, K.M., Hedrich, U.B.S., Masnada, S., Rubboli, G., Gardella, E., Lesca, G., Ville, D., Milh, M., Villard, L. *et al.* (2017) Genetic and phenotypic heterogeneity suggest therapeutic implications in SCN2A-related disorders. *Brain*, **140**, 1316–1336.
12. Satterstrom, F.K., Kosmicki, J.A., Wang, J., Breen, M.S., De Rubeis, S., An, J.-Y., Peng, M., Collins, R., Grove, J., Klei, L. *et al.* (2020) Large-scale exome sequencing study implicates both developmental and functional changes in the neurobiology of autism. *Cell*, **180**, 568–584.e23.
13. Ben-Shalom, R., Keeshen, C.M., Berrios, K.N., An, J.Y., Sanders, S.J. and Bender, K.J. (2017) Opposing effects on $Na_V1.2$ function underlie differences between SCN2A variants observed in individuals with autism spectrum disorder or infantile seizures. *Biol. Psychiatry*, **82**, 224–232.
14. Meisler, M.H., Hill, S.F. and Yu, W. (2021) Sodium channelopathies in neurodevelopmental disorders. *Nat. Rev. Neurosci.*, **22**, 152–166.
15. Planells-Cases, R., Caprini, M., Zhang, J., Rockenstein, E.M., Rivera, R.R., Murre, C., Masliah, E. and Montal, M. (2000) Neuronal death and perinatal lethality in voltage-gated sodium channel αII-deficient mice. *Biophys. J.*, **78**, 2878–2891.
16. Shin, W., Kweon, H., Kang, R., Kim, D., Kim, K., Kang, M., Kim, S.Y., Hwang, S.N., Kim, J.Y., Yang, E. *et al.* (2019) Scn2a haploinsufficiency in mice suppresses hippocampal neuronal excitability, excitatory synaptic drive, and long-term potentiation, and spatial learning and memory. *Front. Mol. Neurosci.*, **12**, 145.
17. Spratt, P.W.E., Alexander, R.P.D., Ben-Shalom, R., Sahagun, A., Kyoung, H., Keeshen, C.M., Sanders, S.J. and Bender, K.J. (2021) Paradoxical hyperexcitability from $Na_V1.2$ sodium channel loss in neocortical pyramidal cells. *Cell Rep.*, **36**, 109483.
18. Léna, I. and Mantegazza, M. (2019) $Na_V1.2$ haploinsufficiency in Scn2a knock-out mice causes an autistic-like phenotype attenuated with age. *Sci. Rep.*, **9**, 12886.
19. Middleton, S.J., Kneller, E.M., Chen, S., Ogiwara, I., Montal, M., Yamakawa, K. and McHugh, T.J. (2018) Altered hippocampal replay is associated with memory impairment in mice heterozygous for the Scn2a gene. *Nat. Neurosci.*, **21**, 996–1003.
20. Ogiwara, I., Miyamoto, H., Tatsukawa, T., Yamagata, T., Nakayama, T., Atapour, N., Miura, E., Mazaki, E., Ernst, S.J., Cao, D. *et al.* (2018) $Na_v1.2$ haplodeficiency in excitatory neurons causes absence-like seizures in mice. *Commun. Biol.*, **1**, 96.
21. Wang, H.-G., Bavley, C.C., Li, A., Jones, R.M., Hackett, J., Bayleyen, Y., Lee, F.S., Rajadhyaksha, A.M. and Pitt, G.S. (2021) Scn2a severe hypomorphic mutation decreases excitatory synaptic input and causes autism-associated behaviors. *JCI Insight*, **6**(15), e150698.
22. Kearney, J.A., Plummer, N.W., Smith, M.R., Kapur, J., Cummins, T.R., Waxman, S.G., Goldin, A.L. and Meisler, M.H. (2001) A gain-of-function mutation in the sodium channel gene Scn2a results in seizures and behavioral abnormalities. *Neuroscience*, **102**, 307–317.
23. Kile, K.B., Tian, N. and Durand, D.M. (2008) Scn2a sodium channel mutation results in hyperexcitability in the hippocampus in vitro. *Epilepsia*, **49**, 488–499.
24. Li, M., Jancovski, N., Jafar-Nejad, P., Burbano, L.E., Rollo, B., Richards, K., Drew, L., Sedo, A., Heighway, J., Pachernegg, S. *et al.* (2021) Antisense oligonucleotide therapy reduces seizures and extends life span in an SCN2A gain-of-function epilepsy model. *J. Clin. Invest.*, **131**(23), e152079.
25. Zhang, J., Chen, X., Eaton, M., Wu, J., Ma, Z., Lai, S., Park, A., Ahmad, T.S., Que, Z., Lee, J.H. *et al.* (2021) Severe deficiency of the voltage-gated sodium channel $Na_V1.2$ elevates neuronal excitability in adult mice. *Cell Rep.*, **36**, 109495.
26. Echevarria-Cooper, D.M., Hawkins, N.A., Misra, S.N., Huffman, A.M., Thaxton, T., Thompson, C.H., Ben-Shalom, R., Nelson, A.D., Lipkin, A.M., George, A.L., Jr. *et al.* (2022) Cellular and behavioral effects of altered $Na_V1.2$ sodium channel ion permeability in Scn2aK1422E mice. *Hum. Mol. Genet.*, **31**(17), 2964–2988.
27. Yang, X.-R., Ginjupalli, V.K.M., Theriault, O., Poulin, H., Appendino, J.P., Au, P.Y.B. and Chahine, M. (2022) SCN2A-related epilepsy of infancy with migrating focal seizures: report of a variant with apparent gain- and loss-of-function effects. *J. Neurophysiol.*, **127**, 1388–1397.
28. Deneault, E., White, S.H., Rodrigues, D.C., Ross, P.J., Faheem, M., Zaslavsky, K., Wang, Z., Alexandrova, R., Pellecchia, G., Wei, W. *et al.* (2018) Complete disruption of autism-susceptibility genes by gene editing predominantly reduces functional connectivity of isogenic human neurons. *Stem Cell Rep.*, **11**, 1211–1225.
29. Lu, C., Shi, X., Allen, A., Baez-Nieto, D., Nikish, A., Sanjana, N.E. and Pan, J.Q. (2019) Overexpression of NEUROG2 and NEUROG1

in human embryonic stem cells produces a network of excitatory and inhibitory neurons. *FASEB J.*, **33**, 5287–5299.
30. Begemann, A., Acuña, M.A., Zweier, M., Vincent, M., Steindl, K., Bachmann-Gagescu, R., Hackenberg, A., Abela, L., Plecko, B., Kroell-Seger, *J. et al.* (2019) Further corroboration of distinct functional features in SCN2A variants causing intellectual disability or epileptic phenotypes. *Mol. Med.*, **25**, 6.
31. Spitzer, N.C. (2006) Electrical activity in early neuronal development. *Nature*, **444**, 707–712.
32. Blankenship, A.G. and Feller, M.B. (2010) Mechanisms underlying spontaneous patterned activity in developing neural circuits. *Nat. Rev. Neurosci.*, **11**, 18–29.
33. Liao, Y., Anttonen, A.-K., Liukkonen, E., Gaily, E., Maljevic, S., Schubert, S., Bellan-Koch, A., Petrou, S., Ahonen, V.E., Lerche, H. *et al.* (2010) SCN2A mutation associated with neonatal epilepsy, late-onset episodic ataxia, myoclonus, and pain. *Neurology*, **75**, 1454–1458.
34. Hanemaaijer, N.A.K., Popovic, M.A., Wilders, X., Grasman, S., Pavón Arocas, O. and Kole, M.H.P. (2020) Ca2+ entry through Na_V channels generates submillisecond axonal Ca2+ signaling. *Elife*, **9**, e54566.
35. Horvath, G.A., Demos, M., Shyr, C., Matthews, A., Zhang, L., Race, S., Stockler-Ipsiroglu, S., Van Allen, M.I., Mancarci, O., Toker, L. *et al.* (2016) Secondary neurotransmitter deficiencies in epilepsy caused by voltage-gated sodium channelopathies: a potential treatment target? *Mol. Genet. Metab.*, **117**, 42–48.
36. Que, Z., Olivero-Acosta, M.I., Zhang, J., Eaton, M., Tukker, A.M., Chen, X., Wu, J., Xie, J., Xiao, T., Wettschurack, K. *et al.* (2021) Hyperexcitability and pharmacological responsiveness of cortical neurons derived from human iPSCs carrying epilepsy-associated sodium channel $Na_V1.2$-L1342P genetic variant. *J. Neurosci.*, **41**, 10194–10208.
37. Hall, C.N., Klein-Flügge, M.C., Howarth, C. and Attwell, D. (2012) Oxidative phosphorylation, not glycolysis, powers presynaptic and postsynaptic mechanisms underlying brain information processing. *J. Neurosci.*, **32**, 8940–8951.
38. Khacho, M., Harris, R. and Slack, R.S. (2019) Mitochondria as central regulators of neural stem cell fate and cognitive function. *Nat. Rev. Neurosci.*, **20**, 34–48.
39. Diets, I.J., van der Donk, R., Baltrunaite, K., Waanders, E., Reijnders, M.R.F., Dingemans, A.J.M., Pfundt, R., Vulto-van Silfhout, A.T., Wiel, L., Gilissen, C. *et al.* (2019) De novo and inherited pathogenic variants in KDM3B cause intellectual disability, short stature, and facial dysmorphism. *Am. J. Hum. Genet.*, **104**, 758–766.
40. Boonsawat, P., Joset, P., Steindl, K., Oneda, B., Gogoll, L., Azzarello-Burri, S., Sheth, F., Datar, C., Verma, I.C., Puri, R.D. *et al.* (2019) Elucidation of the phenotypic spectrum and genetic landscape in primary and secondary microcephaly. *Genet. Med.*, **21**, 2043–2058.
41. Havlicek, S., Kohl, Z., Mishra, H.K., Prots, I., Eberhardt, E., Denguir, N., Wend, H., Plötz, S., Boyer, L., Marchetto, M.C.N. *et al.* (2014) Gene dosage-dependent rescue of HSP neurite defects in SPG4 patients' neurons. *Hum. Mol. Genet.*, **23**, 2527–2541.
42. Sather, W., Dieudonné, S., MacDonald, J.F. and Ascher, P. (1992) Activation and desensitization of N-methyl-D-aspartate receptors in nucleated outside-out patches from mouse neurones. *J. Physiol.*, **450**, 643–672.
43. Schmidt-Hieber, C. and Bischofberger, J. (2010) Fast sodium channel gating supports localized and efficient axonal action potential initiation. *J. Neurosci.*, **30**, 10233–10242.
44. Stuart, T., Butler, A., Hoffman, P., Hafemeister, C., Papalexi, E., Mauck, W.M., III, Hao, Y., Stoeckius, M., Smibert, P. and Satija, R. (2019) Comprehensive integration of single-cell data. *Cell*, **177**, 1888–1902.e21.
45. Krämer, A., Green, J., Pollard, J., Jr. and Tugendreich, S. (2014) Causal analysis approaches in ingenuity pathway analysis. *Bioinformatics*, **30**, 523–530.
46. Hallermann, S., de Kock, C.P.J., Stuart, G.J. and Kole, M.H.P. (2012) State and location dependence of action potential metabolic cost in cortical pyramidal neurons. *Nat. Neurosci.*, **15**, 1007–1014.